FINITE ELEMENT MODELING OF REINFORCED MASONRY SHEAR WALLS UNDER SEISMIC LOADS

Alireza Sayah [1], Andreas Stavridis [2], Jacob D. Sherman[3] and David I. McLean [4]
[1] PhD student, Department of Civil Engineering, University of Texas at Arlington, Arlington, TX 76019, USA, alireza.sayah@mavs.uta.edu
[2] Assistant Professor, Department of Civil Engineering, University of Texas at Arlington, Arlington, TX 76019, USA, stavridis@uta.edu
[3]Walker Structural Engineering, LLC, Bend, OR 97701, USA, jacob.sherman@email.wsu.edu
[4] Professor, Department of Civil and Environmental Engineering, Washington State University, Pullman, WA 99164, USA, mclean@wsu.edu

ABSTRACT
This paper presents a finite element scheme that combines the smeared and discrete crack approaches to simulate the behavior of reinforced masonry shear walls under in-plane lateral loads. The smeared crack elements are used to capture the crushing and diffused cracking of masonry, while the zero-thickness interface elements are employed to allow the development of discrete dominant cracks along the bed and head joints, as well as in the concrete masonry units. The proposed scheme has been evaluated with experimental data obtained from tests of two fully-grouted reinforced masonry shear wall specimens. The material parameters have been calibrated with data from material tests and data available in the literature. The comparison of the numerical results obtained from the finite element analyses and the experimental data indicates that the finite element models can simulate the failure patterns of their experimentally tested counterparts including crushing and the development of shear and flexural cracks. The finite element model can also capture reasonably well the initial stiffness, the peak resistance, and the residual strength of the specimens.

KEYWORDS: reinforced masonry, shear wall, seismic performance, finite element modeling

INTRODUCTION
Reinforced masonry structures are constructed from a variety of materials including concrete masonry units (CMU), mortar, grout and steel reinforcement. The interaction and nonlinear response of these materials to seismic loads makes the analytical modeling of the performance of such structures rather challenging. A variety of techniques have been used to model the behavior of reinforced masonry structures [1-4], with different levels of accuracy. Most commonly, researchers have used smeared crack elements to model the masonry walls. However, the use of these elements has some limitations that can affect the results of the analysis. The most common limitation is the stress-locking problem [5] caused by the unrealistic kinematic constraint introduced by smeared crack elements. As a result of stress locking, smeared crack elements are unable to capture the brittle behavior of an actual specimen following the development of shear cracks. Hence, the analysis can lead to unconservative results. Moreover, the use of smeared crack elements is associated with an issue known as mesh-size sensitivity [6,7]. To circumvent these deficiencies in models of similarly brittle materials such as concrete, researchers have used the discrete crack approach in conjunction with the smeared crack approach [5,8].

In this study, a similar approach has been adopted to develop a finite element modeling scheme to simulate the performance of reinforced masonry shear walls under lateral loads. The proposed model combines the smeared and discrete crack approaches to allow the development of discrete and diffused shear and flexural cracks. The scheme has been evaluated with data obtained from tests of two fully-grouted masonry shear walls conducted at the Washington State University (WSU) [9] as a part of a collaboration research project including researchers from University of California San Diego (UCSD) and University of Texas (UT) at Austin as well. The comparison of the experimental and numerical results indicates that the models can predict well the initial stiffness, peak load, and residual strength. The models can also capture the failure patterns of the physical specimens.

FINITE ELEMENT MODELING SCHEME

The modeling scheme proposed in this study for the reinforced masonry shear walls is presented in Figure 1. As shown in the figure, each CMU is modeled as a module discretized in two main segments. Each segment consists of four triangular smeared crack elements that are inter-connected with four diagonal interface elements. Moreover, horizontal and vertical interface elements representing bed and head joints surround the module and are used to connect the module to the adjacent CMUs. As a result, discrete cracks can develop at angles of 0°, 90°, and ±θ where θ depends on the unit geometry. For the dimensions of the typical units, θ is 45°; hence, the interface element can represent diagonal shear cracks. In the actual units, the two segments are connected with the web that is unlikely to crack. However, a vertical interface element is used in the model. This element could be eliminated, but it is used here to maintain the consistency of the modeling scheme across the height of the structure. The element is calibrated so that it has high stiffness and it remains elastic at all times.

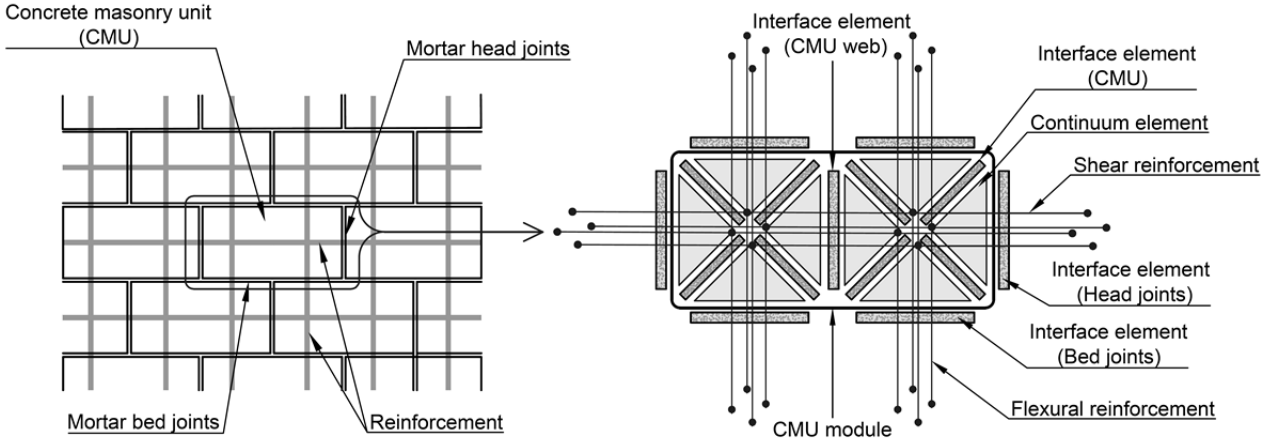

Figure 1: Proposed finite element scheme for reinforced masonry walls.

As shown in Figure 1, each flexural and shear reinforcing bar is equally divided into four truss elements attached to interior nodes of the triangular smeared crack elements. This arrangement permits the placement of steel reinforcement at locations similar to those in the actual structure. Moreover, this arrangement ensures that the right amount of flexural and shear reinforcement is crossed by all possible discrete cracks.

CONSTITUTIVE MODEL FOR SMEARED-CRACK ELEMENTS

The smeared crack model used in this study was developed by Lotfi and Shing [1] and it has been implemented in the Finite Element Analysis Program (FEAP) [10]. For the uncracked material, the model adopts an elastic-plastic law based on the von Mises yield criterion and an associated flow rule. This is combined with a Rankine-type tension cut-off criterion. As illustrated in Figure 2(a), a parabolic function followed by an exponential function is used to relate the effective stress, σ_e, to the effective plastic strain, ε_p and define the strain hardening/softening behavior. The von Mises criterion is expressed as:

$$J_2 - \frac{1}{3}\sigma_e^2\left(\varepsilon_p\right) = 0 \tag{1}$$

where J_2 is the second invariant of the deviatoric stress tensor.

Cracking due to tension is initiated when the maximum principal stress reaches the tensile strength, f_t', as illustrated in Figure 2(b). Subsequently, cracks are assumed to initiate in the direction normal to the direction of the maximum principal stress. The material model then adopts an orthotropic material law to simulate the nonlinear behaviors in tension and compression. In this model, the axes of orthotropy, t-n, are fixed and they are normal and tangential to the direction of the crack. As shown in Figure 2(c), an exponential decaying curve is used to model the softening behavior in tension. The compressive behavior of the cracked material is expressed as a parabolic function followed by an exponential function, shown in Figure 2(d). The plasticity and orthotropic laws need to be consistently calibrated to allow a smooth transition from the former to latter model upon crack initiation. More information about the constitutive models can be found in [1].

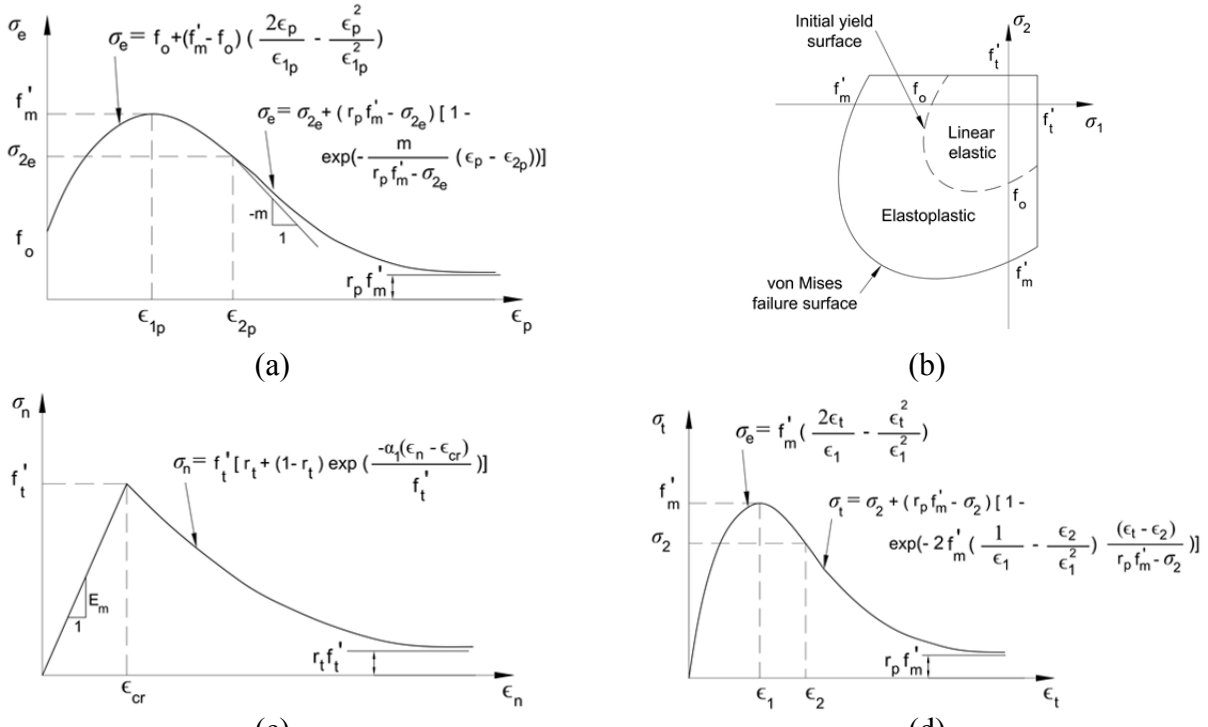

Figure 2: Smeared crack constitutive model: (a) effective stress-vs.-effective plastic strain relation for plasticity model, (b) failure surface for plasticity model, (c) tensile behavior of orthotropic model, and (d) compressive behavior of orthotropic model.

DILATANT INTERFACE MODEL

The interface model used in this study is an elastic-plastic model developed by Lotfi and Shing [2]. This model is implemented in FEAP as a four-noded, zero-thickness, isopararametric line element, which is illustrated in Figure 3(a). The constitutive model uses a cohesive crack formulation and simulates Mode-I and Mode-II fracture, as well as the mixed-mode fracture due to the interaction of axial and shear stresses. The model accounts for the shear dilation, which is often observed in laboratory tests and can be important for the simulation of the shear response of a confined crack. To model fracture, the following hyperbolic yield function is used:

$$F(\sigma, q) = \tau^2 - \mu^2(\sigma - s)^2 + 2r(\sigma - s) = 0 \tag{2}$$

in which μ is the slope of the asymptote of the hyperbola; s is the tensile strength; and r is the radius of the yield surface at the vertex of the hyperbola shown in Figure 3(b). The variable $q = \{s \quad r \quad \mu\}^T$ describes the evolution of the yield surface with $q_0 = \{s_0 \quad r_0 \quad \mu_0\}^T$ defining the initial yield surface, while $q_r = \{0 \quad r_r \quad \mu_r\}^T$ defines the final state. A non-associated flow rule with the following plastic potential is used to limit the excessive dilation:

$$Q(\sigma, q) = \eta\tau^2 - (r - r_r)(\sigma - s) \tag{3}$$

in which η is a parameter scaling the shear dilatation.

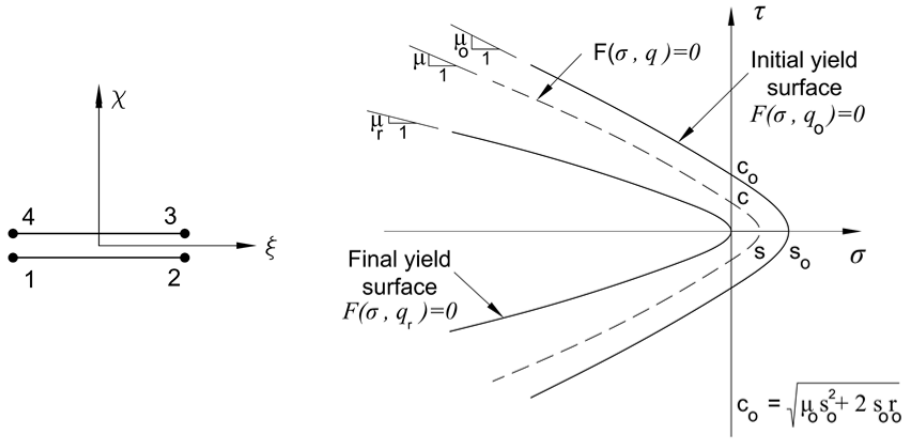

(a) (b)

Figure 3: Isoparametric interface element: (a) geometry and (b) hyperbolic yield criterion.

CALIBRATION OF MATERIAL MODELS

The calibration of the model should be done in a consistent manner. To this end, one can first calibrate the interface elements. As illustrated in Figure 1, there are three groups of interface elements in the model including the vertical elements inter-connecting the two segments of the CMU, the diagonal elements inside each segment, and the horizontal and vertical elements connecting the different CMU units. The first group of elements coincides with the CMU webs. Since no cracking is anticipated in these locations, the strength or thickness of these elements should be large enough to ensure these elements remain elastic and that they do not affect the structural behavior. The second group of elements are used to allow the development of diagonal

cracks in the CMU units while the last group of elements can simulate cracks in the bed and head joints around the masonry units. In fully grouted walls, the crack behavior for these two groups of elements would be dominated by the grout. Hence, the difference in strength between cracks propagating through the masonry units and cracks propagating at the location of the joints can be ignored for simplicity given the lack of data that can allow the exact estimation of this difference. As a consequence, the same material properties are assigned to both types of cracks.

Since the interface elements represent cracks, they should have no or small influence on the structural behavior prior to cracking. Therefore, they are elastic with a high stiffness. However, the stiffness should not be too high to make the model numerically ill-conditioned [8]. One can assess the influence of these elements on the structural behavior by comparing the compressive behavior of one segment from Figure 1 to that of a single quadrilateral element of the same overall dimensions. Tests to assess the tensile properties of masonry are difficult to conduct. In the absence of test data, the tensile strength of masonry, f_t', can be assumed to be 10% of the compressive strength of prism [11]. The post cracking behavior of the masonry can be defined by determining the Mode-I and Mode-II fracture energies, G_f^I and G_f^{II}. Estimating the Mode-II fracture energy is difficult. However, it has been found [14] that assuming $\mathrm{G_f^{II}} = 10\mathrm{G_f^{I}}$ can provide satisfactory results and this relation is used in this study. One should also define the parameters $q_0 = \{\mathrm{s_0} \quad r_0 \quad \mu_0\}^T$ and $q_r = \{0 \quad r_r \quad \mu_r\}^T$ that define the initial and final yield surfaces, and the parameter η that scales the dilatancy. Experimental data from shear tests on grouted masonry are not readily available; hence data from mixed-mode fracture tests for concrete have been used to calibrate these parameters in this study [15].

With these assumptions one can calibrate the behavior of the interface element. The tensile properties of the smeared-crack elements can be then calibrated using the stress-displacement curve of the interface model as a reference. To compare the curves obtained by the two models, one can convert the tensile strain obtained from a smeared-crack element to displacement by means of a characteristic length. For constant strain triangular elements, which are used in the proposed scheme, the characteristic length can be assumed to be equal to the square root of the element area [16]. For the calibration of the compressive behavior of smeared-crack elements, data obtained from compressive tests of grouted prisms can be used. Since the model uses both plasticity and orthotropic models, one can first calibrate the orthotropic model by defining the parameters f'_m, ε_1, and ε_2, and then calibrate the plasticity model accordingly to ensure a smooth transition from the latter to the former upon crack initiation.

VALIDATION OF THE MODELING SCHEME

The proposed scheme is used to model two fully-grouted, cantilever reinforced masonry shear walls subjected to in-plane cyclic loads. The two specimens considered here were part of an extensive experimental program conducted at Washington State University [9]. Figure 4 illustrates the typical test setup and specimen details. The walls were constructed of CMUs with nominal dimensions of 203×203×406-mm (8×8×16-in). The walls were reinforced for flexure with No.4 bars placed vertically every 203mm (8 in.) on center. The shear reinforcement was also placed every 203mm (8 in.) on center and included 180° hooks at each end that were placed around the extreme flexural reinforcement in accordance with 2008 MSJC Building Code Requirements for Masonry Structures [17]. In the specimens, flexural reinforcement was spliced at the wall base with 406 mm (16 in)-long lap splices according to MSJC Code requirements of

the walls. Since the MSJC splice requirement were met in the experimental tests, it is assumed that the perfect transfer of the tensile stresses along the height of the splice exists. Hence, for simplicity, in the models, splice is treated as only one reinforcing bar instead of a combination of starter bar and the longitudinal bar. Additional details on the design and testing of the walls can be found in [9]. Two reinforced concrete beams were placed at the top and bottom of the specimens to apply the lateral and vertical loads, anchor the vertical reinforcement, and also attach the specimens to the strong floor. The design details for the two masonry walls used for the model validation are summarized in Table 1.

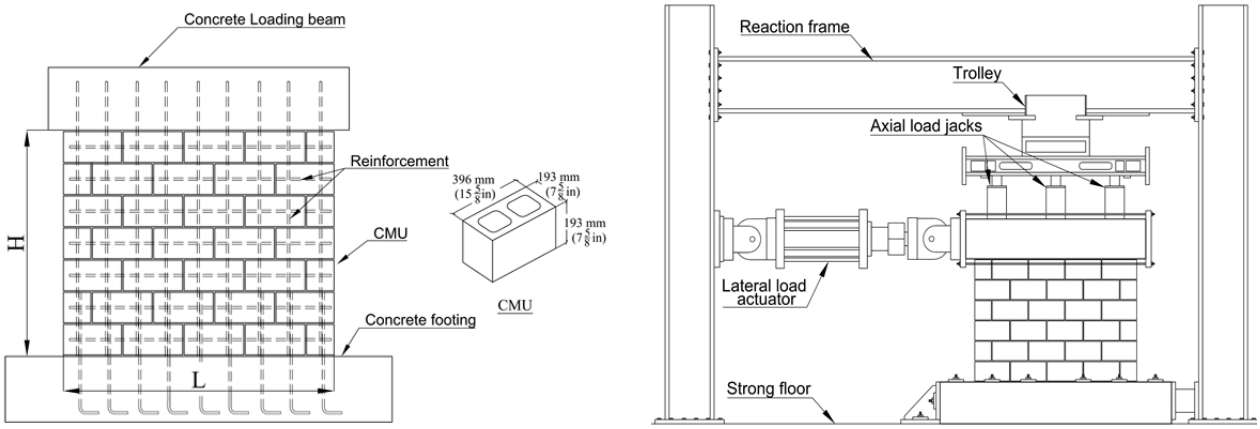

(a) (b)

Figure 4: Details of: (a) specimen design and (b) test setup.

The two specimens are modeled using the proposed scheme shown in Figure 1. Since no cracks are expected to develop in the concrete beams at the top and bottom of the wall, these are modeled with four-noded linear elastic elements for computational efficiency. In the absence of data for the Mode-I fracture energy, G_f^I, of the fully grouted masonry, one can estimate its value using available data in the literature for concrete of similar strength. Such data for concrete mixes of different strengths can be found in [12] and [13]. Hence, considering the average compressive strength of 20.96 MPa (3.04 ksi) for the grouted prisms [9], the Mode-I fracture energy, G_f^I, is assumed to be 140 N/m (0.0008 kips/in). The Mode-II fracture energy is accordingly calculated by assuming $G_f^{II} = 10G_f^I$ [14]. The values of the material parameter used for calibration of the interface and smeared-crack elements simulating the behavior of masonry are summarized in Table 2. The calibrated curves for the smeared crack and interface elements in tension and compression are illustrated in Figure 5. The steel was modeled as elastic-perfectly plastic with yield strength of 453.3 MPa (65.75 ksi).

Table 1: Specimen design details and material properties.

Specimen	Wall Dimensions, H × L mm (in)	Axial Load Ratio $(\frac{P}{f'_m A_g})$	Flexural Reinforcement * mm (in) **	Shear Reinforcement * mm (in)	f'_m, MPa (ksi)
4	1626×1845 $(64 \times 71\,5/8)$	0.0625	#4 @ 203 (8 in)	#4 @ 203 (8 in)	20.96 (3.04)
6	1219×1845 $(48 \times 71\,5/8)$	0.0625	#4 @ 203 (8 in)	(2) #4 @ 203 (8 in)	

* The average yield strength for #4 reinforcement is 453.3 MPa (65.75 ksi).

** Diameter of #4 bar is 12.7 mm (0.5 in).

Table 2: Material parameters for interface and smeared crack elements.

Smeared-crack			Interface element								
f'_m MPa (ksi)	ε_1	ε_2	D_n GPa/m (ksi/in)	f'_t MPa (psi)	G_f^I N/m (kips/in)	G_f^{II} N/m (kips /in)	μ_0	μ_r	r_0 MPa (Ksi)	r_r MPa (Ksi)	η
29.6 (3.04)	0.004	0.0049	1764 (6500)	2.96 (0.304)	140 (0.0008)	1400 (0.008)	1	0.7	0.34 (0.05)	0.034 (0.005)	0.6

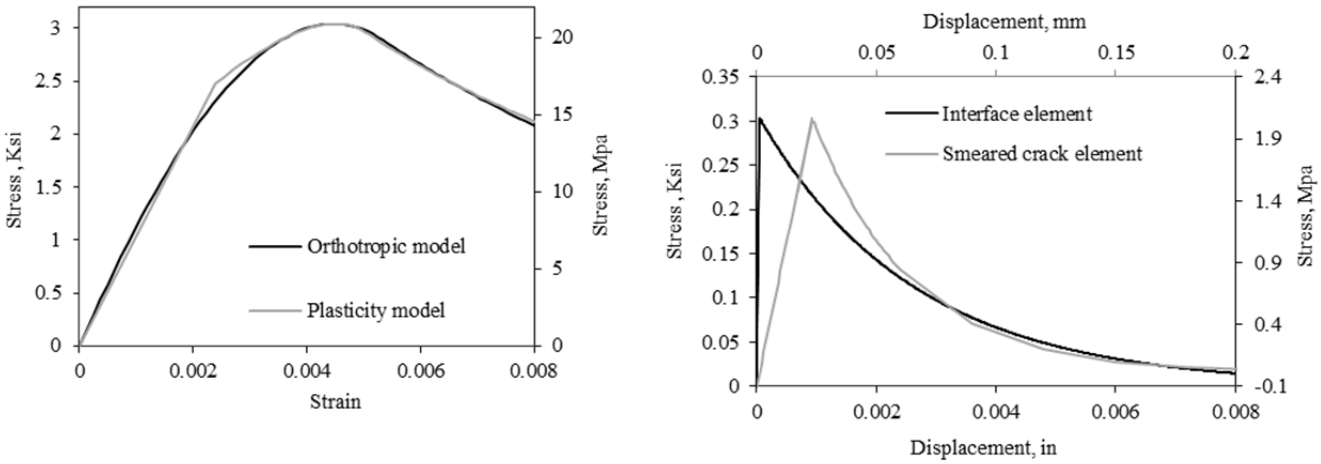

(a) (b)

Figure 5: Calibration of smeared crack and interface elements: (a) compressive behavior; (b) tensile behavior.

NUMERICAL RESULTS

Although the test specimens were subjected to a cyclic loading sequence, monotonic analyses have been used in this study to model the behavior of the walls. Furthermore, since the geometry of the test specimens is symmetric, a single analysis is used to represent the structural performance in both loading directions. The load-vs.-displacement curves obtained from the finite element analyses are compared with the experimental results in Figure 6.

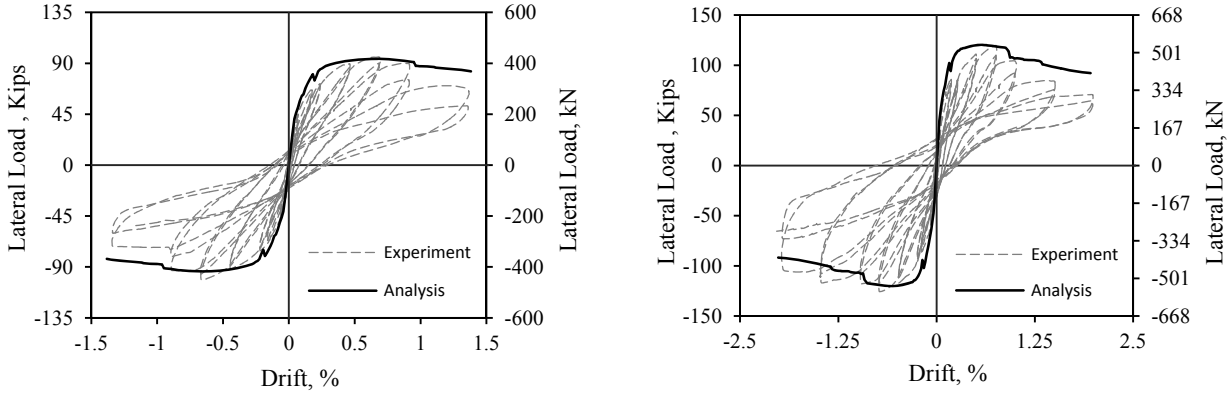

(a) (b)

Figure 6: Experimental and analytical lateral load-vs.-drift curves: (a) Specimen 4; (b) Specimen 6.

Specimen 4

The load-vs.-displacement curve obtained from the finite element model of Specimen 4 matches well the experimental one, as shown in Figure 6(a). More specifically, the model captures the initial stiffness, the peak load, and the drift at peak load, but overestimates the residual strength in both directions. Figure 7 shows the deformed shape and the damage patterns of the analytical model and the test specimen failure patterns at 1.35% drift. The reinforcement is not shown in the figure to enhance its visual clarity. The crushing of a smeared-crack element is denoted by an "X," and the cracking by a line reflecting the crack orientation. The length of these lines corresponds to the extent of crushing or crack opening respectively. The behavior of the specimen was dominated by flexure with small levels of shear cracking in the bottom three courses. In the specimen, at the instant of peak load, all of the tensile vertical reinforcement at the base of the wall experienced yielding that confirms the model results. Moreover, the model captures the toe-crushing of the walls, as well as the diffused flexural cracks in the windward side of the walls and the diagonal shear cracks observed in the bottom courses of the test specimen.

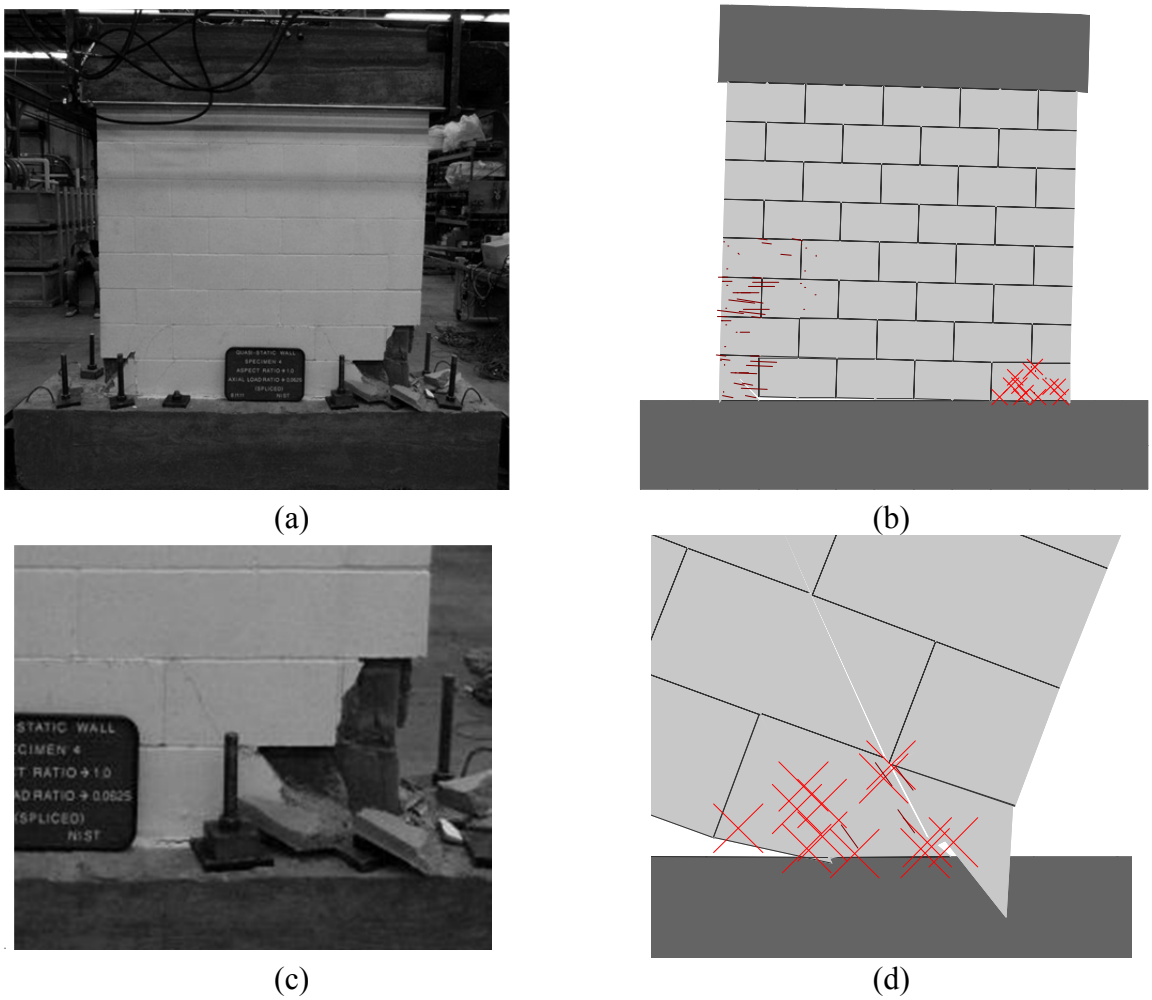

(a) (b)

(c) (d)

Figure 7: Failure patterns for Specimen 4: (a) laboratory specimen at the end of test and (b) analytical model deformed shape a lateral drift of 1.35% drift; c) toe crushing of specimen; d) close-up of the analytical model.

Specimen 6

The load-vs.-displacement curves obtained from the finite element analysis are compared with the experimental results in Figure 6(b). As shown in the figure, the numerical model matches the behavior of the specimen in the negative direction very well. However, the response of the specimen is not symmetric; hence, the model tends to overestimate the strength of the specimen in the positive direction in terms of residual strengths. Moreover, the drifts at the peak load and the onset of toe crushing obtained from the analysis are smaller than those obtained from the experiment. Moreover in the model at the instant of peak load, all the rebars located the base of the wall experienced yielding that confirms with the experimental test data obtained from strain gages attached to the rebars. Figure 8 shows the deformed shape from the analytical model and the test specimen failure patterns at 2.00% drift which was the largest drift imposed on the specimen during the test. In the experimental test, the wall behavior was dominated by flexure, but diagonal shear cracks were observed in every course. This behavior was accurately captured by the finite element mode as demonstrated in Figure 8(b).

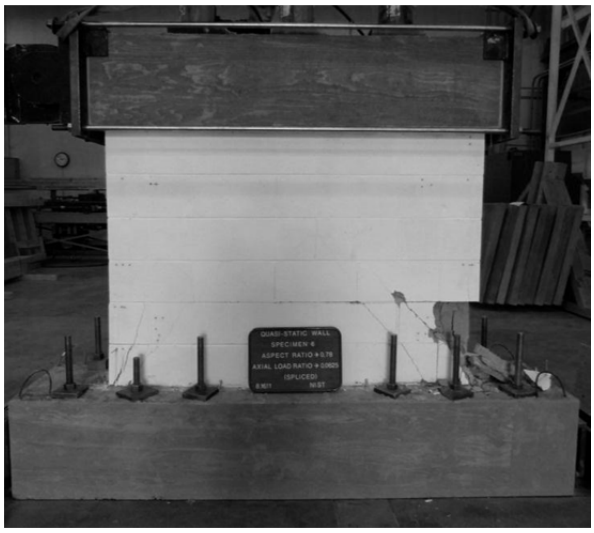

(a)

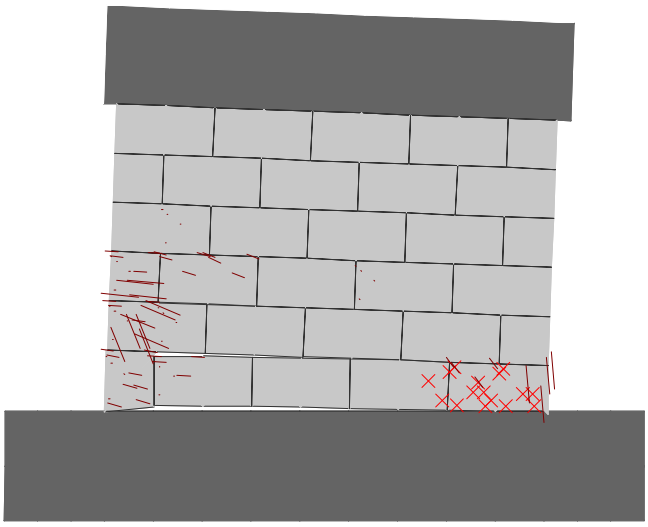

(b)

(c)

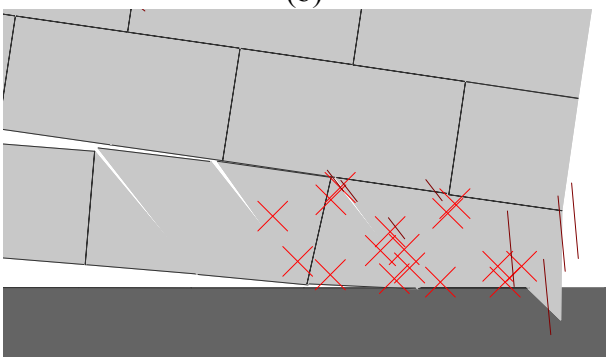

(d)

Figure 8: Failure patterns for Specimen 6: (a) laboratory specimen at the end of test; (b) analytical model deformed shape a lateral drift of 2.00% drift; (c) close-up of the toe crushing and cracking of Specimen 6; (d) close up of the toe crushing and cracking of the analytical model.

CONCLUSIONS

This paper presents a finite element scheme that combines the smeared and discrete crack approaches for modelling the behavior of reinforced masonry shear walls. The model is calibrated with a rigorous procedure using test data and data available in the literature for concrete of similar strength. The proposed modelling methodology has been used to simulate the performance of two fully grouted masonry shear walls tested in the Washington State University. The comparison of the numerical and experimental results indicates that the models are able to accurately predict the failure patterns of the specimens. The introduction of the zero-thickness interface elements to the modelling scheme eliminates potential numerical issues that models with smeared crack elements only could face. Moreover, the scheme allows the precise modelling of the steel reinforcement with discrete bars that are the same locations as in the actual specimens.

In terms of the predictive capabilities, the finite element models capture not only the crushing at the bottom corners of the walls, but also the development of flexural and shear cracks throughout the wall. Moreover, the models predict well the initial stiffness and peak load of the walls. However, the predicted values for the residual strength slightly differ from the experimental tests values. This can be expected considering the highly nonlinear behavior of the walls, the lack of experimental data for the calibration of the material models, and the non-symmetric behavior of Specimen 6. Material tests on masonry assemblies would be very useful in producing data for the more accurate calibration of the numerical models.

ACKNOWLEDGEMENTS

The authors would like to thank the Dr. Benson Shing of the University of California San Diego, Dr. Richard Klingner, and Dr. Farhad Ahmadi of the University of Texas, Austin for their valuable contribution during the course of this study. However, opinions expressed in this paper are those of the authors and do not necessarily represent those of the aforementioned collaborators.

REFERENCES

1. Lotfi, H. R., and Shing, P. B. (1991). “An appraisal of smeared crack models for masonry shear wall analysis.” J. Computers Struct., 120(1), 63–80.
2. Lotfi, H. R., and Shing, P. B. (1994). “An interface model applied to fracture of masonry structures.” J. Struct. Eng., 120 (1), 63–80.
3. El-Dakhakhni, W., Drysdale, R., and Khattab, M. (2006). ”Multilaminate Macromodel for Concrete Masonry: Formulation and Verification.” J. Struct. Eng., 132(12), 1984–1996.
4. Haach, V. G., Vasconcelos, G., and Lourenço, P. B. (2011) “Parametrical study of masonry walls subjected to in-plane loading through numerical modeling.” J. Engineering Struct., 33(4), 1377–1389.
5. Rots, J. G. (1988). “Computational modeling of concrete fracture.” Ph.D. dissertation, Delft Univ. of Technology, The Netherlands.
6. Bažant, Z. P., and Cedolin, L. (1979). “Blunt crackband propagation in finite element analysis.” J. Engrg. Mech. Div., ASCE, 105 (2), 297–315.97a.
7. Bazant, Z. P., and Oh, B. H. (1983). “Crack band theory for fracture of concrete.” Mater. Struct., 16(93), 155–177.

8. Stavridis, A. and Shing, P. (2010). “Finite-element modeling of nonlinear behavior of masonry-infilled RC frames.” J. Struct. Eng., 136(3), 285–296.
9. Sherman, J. D. (2011). “Effects of key parameters on the performance of concrete masonry shear walls under in-plane loading” M.Sc. thesis, Washington State University, Pullman, WA.
10. Taylor, R. L. (2007). FEAP—A Finite Element Analysis Program. Version 8.1. University of California at Berkeley.
11. Drysdale, R. G., and Hamid, A. A. (2008). “Masonry structures-behavior and design.” The Masonry Society.
12. Bazant, Z. P., and Becq-Giraudon, E. (2002). “Statistical prediction of fracture parameters of concrete and implications for choice of testing standard.” Cem. Concr. Res., 32, 529–556.
13. Wittmann, F. H. (2002). “Crack formation and fracture energy of high strength concrete.” SAPSER, 27(4), 413–423.
14. Lotfi, H. R. (1992). “Finite element analysis of fracture of concrete and masonry structures.” Ph.D. dissertation, Univ. of Colorado at Boulder.
15. Hassanzadeh, M. (1990). “Determination of fracture zone properties in mixed mode I and II.” Eng. Fract. Mech., 35(4–5), 845–853.
16. Papadrakakis, M., Papadopoulos, V., Georgioudakis, M., Hofstetter, G., and Feist, C. (2005). “Reliability analysis of a plain concrete beam.” IALAD Project Rep., Verbund-Austrian Hydro Power, Austria.
17. Masonry Standards Joint Committee (MSJC). (2008). Building Code Requirements for Masonry Structures.” TMS 402/ACI 530/ASCE 5, American Concrete Institute, Farmington Hills, MI., American Society of Civil Engineers, Reston, VA and The Masonry Society, Boulder, CO.